Fundamental Mechanisms in Orthogonal Cutting of Medical Grade Cobalt Chromium Alloy (ASTM F75)

Eamonn Ahearne*, Szymon Baron[1,*]

Abstract

Cobalt chromium (Co-Cr-Mo) alloys are sui generis materials for orthopaedic implants mainly due to the unique properties of biocompatibility and wear resistance in the demanding in vivo environments. Notwithstanding the importance of the machining processes, a review of literature in the public domain has identified a niche for research into the fundamental mechanisms in cutting of Co-Cr-Mo alloys.

This paper reports on initial research into cutting of the biomedical grade cobalt chrome molybdenum (Co-Cr-Mo) alloy, ASTM F75. Following an initial review of the known micro-structural, physical and mechanical properties of the class of Co-Cr-Mo alloys, the results of a full factorial, orthogonal cutting experiment are presented. This involved measurement of force components (F_f and F_t) as a function of the undeformed chip thickness (h) and cutting speed (v_c) which were varied over ranges from 20 to 140 μm and 20 to 60 m/min respectively. The results demonstrated an expected linear increase in force components with h at speeds of 20 and 60 m/min. However, at the intermediate speed of 40 m/min, there was a transition between about 60 and 80 μm indicating a discontinuous rather than continuous effect of speed.

The results enabled determination of the cutting force coefficients K_{tc}, K_{te}, K_{fc} and K_{fe}, for the ranges examined as well as the coefficients, $k_{i1.0.1}$ and $m_{i0.1}$, of the Kienzle equations. These relations will enable macro-mechanic modelling of more complex cutting operations, such as milling, in the future.

Keywords: Machining, Cobalt Chromium, Orthogonal Cutting, Cutting Forces

1. Introduction

Cobalt chromium (Co-Cr-Mo) alloys are sui generis materials for components of orthopaedic implants due mainly to the unique properties of biocompatibility and wear resistance in the demanding in vivo environment. Other commonly used biomedical materials for orthopaedic implants are medical grade titanium alloy (Ti-6Al-4V) and ultra-high molecular weight polyethylene (UHMWPE) (1). Figure 1 shows the main components of a "total knee arthroplasty (TKA)" assembly, where two of the three components are in a Co-Cr-Mo alloy conforming to the ASTM F75 material standard. The increasing demand for this alloy is related to the market demand for orthopaedic implants. For example, the number of total knee arthroplasty procedures in the USA in 2008 was ≈ 650,000 with a recorded compound annual growth rate (CAGR) of 7.9 % between 1997 and 2008 (3). A more recent study shows the US market for hip implants valued at $2.77 Bn. in 2011, involved ≈ 471,000 hip implant procedures, with predicted increases of 175% in hip replacements and 673% increase TKA procedures by 2030 (3). The increase in CAGR is

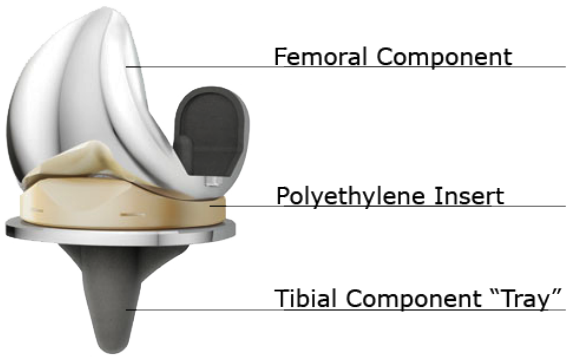

Figure 1: Main components of a TKA. (2)

*School of Mechanical and Materials Engineering, University College Dublin (UCD), Ireland
[1]Tel:+353 (0)1 716 1993 szymon.baron@ucdconnect.ie

primarily attributed to (a) extended life expectancy, (b) increased physical activity, (c) raising levels of obesity (4).

The Co-Cr-Mo components of orthopaedic implants are machined from near-net shape investment cast or forged forms in a process chain that is determined by the final features and dimensions, as well as the exacting specifications for tolerances, surface finish and integrity (5). Importantly, these machining processes affect the characteristics of the functional surfaces of the components (6, 7) and potentially have incipient effects on the life cycle performance, where such surfaces are subjected to high levels of tribo-mechanical stress in the bio-milieu. Given the importance of mechanical cutting processes (both defined and undefined edge) in this process chain, it is surprising that there has been little published research, either applied or of a more fundamental nature.

The objective of this research is to report on initial results of investigation into the fundamental mechanisms in cutting of the cobalt chromium alloy conforming to the ASTM F75 standard. Specifically, this paper will describe the effects of control parameters: v_c and h on the resulting feed F_f and thrust F_t components in orthogonal cutting experiment. This is followed by determination of the cutting coefficients K_{tc}, K_{te}, K_{fc} and K_{fe} as well as $k_{i1.0.1}$ and $m_{i0.1}$ of the Kienzle equation to provide the basis for future analysis of forces in a wide range of cutting operations (milling, drilling, broaching etc.). The structure of this paper is determined by the general objective of elucidation of the fundamental mechanisms in cutting of Co-Cr-Mo alloys with a focus on the ASTM F75 grade. Thus, a description of Co-Cr-Mo alloys is first provided referring to composition, microstructure, physical and mechanical properties. With reference to these properties, and previous work by the authors (8, 9), definitions of "machinability" are considered and a comparison made between Co-Cr-Mo alloys and other "difficult-to-cut (DTC)" materials. This provides a basis for the present research and specifically the design of experiments and the experimental set-up to compare ASTM 75 with the "DTC" biomedical titanium alloy, ASTM F136 Ti-6Al-4V. Presentation of the results of a full factorial experiment design is followed by analysis, discussion and conclusions on the main hypotheses and knowledge generated by the reported research.

2. Literature Review

2.1. Material Science / Metallography

Cobalt Chromium alloys were originally studied by Haynes in 1907 (5) who referred to the alloys of this binary as "stellite" (from the Latin "stella" for star) due to the stainless nature and "star-like" lustre (10). Co-Cr-Mo alloys exhibit a two phase dendritic solidification process. Dendritic regions are nobler, rich in cobalt (γ-phase) and have a face-centred-cubic (FCC) structure. Interdendritic regions are the less noble phase with a hexagonal-close-packed (HCP) structure (11). An equilibrium diagram, developed for the Co-Cr-Mo binary, is shown in Figure 2 indicating the microstructural changes under thermodynamic equilibrium conditions (12). Table 1 shows the composition of two

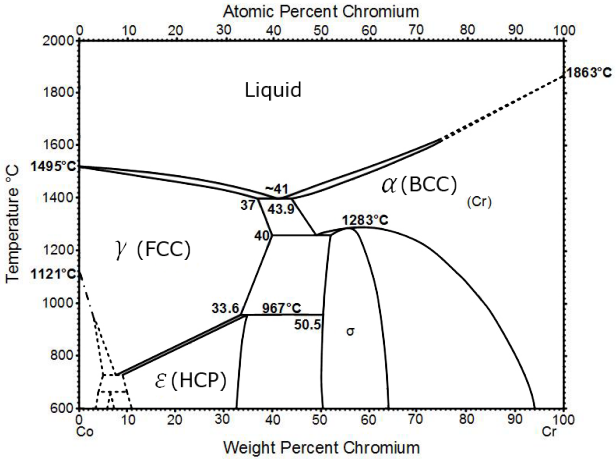

Figure 2: Phase diagram of binary Co-Cr-Mo alloy. (12)

ASTM grades used for orthopaedic implants, where Co is the base metal and Cr and Mo are the primary alloying elements. The presence of chromium provides the high resistance to wear and corrosion through the formation of a hard passivation layer of chromium (III) oxide (Cr_2O_3).

Increasing the chromium content also promotes the formation of hard carbides which increases the alloys strength (13). These carbides are found to: These carbides are found to:

(a) Disperse in the matrix, increasing the strength of the alloy,

(b) Precipitate at the grain boundaries suppressing gross sliding and dislocation migration (5).

Due to the large atomic size, alloying with Mo (or W) further strengthens the alloy. In large quantities Mo (or W) also forms carbides and precipitate as M_6C (16). Phase precipitation is considered the primary strengthening mechanism in the Co-Cr-Mo systems. Ni stabilises the FCC phase by suppressing FCC to HCP transformation of Co at low temperature (17). FCC structures are characterised by high work hardening

Element	Co	Cr	Mo	C	Si	Mn	Fe	Ni
ASTM F75(14)	*Bal.*	27.0 – 30.0	5.0 – 7.0	< 0.35	< 1.0	< 1.0	< 0.75	< 0.5
ASTM F1537(15)	*Bal.*	27.8	5.5	0.05	0.25	0.68	0.25	0.31

Table 1: Chemical composition of ASTM F75 and ASTM F1537 Co-Cr-Mo alloys

rates and can absorb stress by FCC to HCP transformation (13, 18). Therefore, Ni improves the mechanical properties of the alloy, however its content must be limited as Ni is one of the most common sensitizers in human body (19). As-cast F75 Co-Cr-Mo is characterised by a dendritic FCC cobalt base matrix with secondary phase at grain boundaries and at interdendritic zones (11). Thermo-mechanical treatments such as: solution treatment (ST), partial solution treatment (PST) or hot isostatic pressing (HIP) can be applied to refine the microstructure of the alloy and improve its mechanical properties (13). Short dendritic arm spacing and small grain size improve strength while large grain size improves ductility of the alloy (13). HIP treatment reduces the level of porosity originating in the solidification process and thereby sites for crack initiation, propagation and effective strength reduction (20). Dendritic structures of Co-Cr-Mo become indistinct after heat treatment, see Figure 3.

2.2. Material Properties and Machinability

Clearly, the material composition and micro-structure affect the mechanical properties. Table 2 shows the main properties at ambient for the three materials referred to in this paper including two investigated in previous research work by the authors (8, 9). The CoCr ASTM F1537 alloy is a wrought Co-Cr-Mo alloy, supplied and certified by Sandvik, modified by "warm working" after casting. The table also shows a medical grade titanium alloy, Ti-6Al-4V ASTM F136, which is used as a baseline difficult-to-cut (DTC) material; the property values are the "typical" values provided on the Sandvik website (21). The physical and mechanical properties shown in the table 2 are limited as predictors of performance in cutting, as the values are determined under ambient conditions, while the properties that affect the response variables in cutting vary as a function of the extreme temperatures, strains and strain rates. Nor are the properties shown in the table directly useful for defining machinability, or by corollary a difficult-to-cut (DTC) material, given alone the number of different definitions, and the implicit measures of a DTC, some more subjective and less quantifiable than others.
For example, the basic definition of machinability proposed by Shaw (23) employs three measures namely (1) tool life (2) surface finish and (3) power required to cut. Clearly all these measures are functions of many material, tool, machine, control and process parameters. Considering the "power required to cut", which is of interest here, it would be expected that the following properties from table 2 would determine the levels of power in cutting on a first order basis:

(a) the yield strength (σ_y) or, more exactly, the flow stress which is a function of strain, strain rate and temperature as expressed in a number of empirical and semi-empirical models, for example, the ubiquitous Johnson-Cook flow stress model.

(b) the friction coefficient applying at the interface of the tool-work which is dependent on the tool-work counterface materials and global-local application-specific process parameters (for example, coolant parameters) (23) Thus, obtaining comparative values for the friction coefficient is not trivial and is not available and therefore not shown in table 2.

(c) the thermal diffusivity (α) which, by definition, is related to the material density, conductivity and specific heat capacity as follows;

$$\alpha = \frac{k}{\rho \cdot c_p} \tag{1}$$

Where, k is thermal conductivity ($W.m^{-1}.K^{-1}$), ρ is density ($kg.m^{-3}$) and c_p is specyfic heat capacity ($J.kg^{-1}.K^{-1}$).
Clearly, the thermal diffusivity affects the temperature in the cutting zone and therefore the many temperature-dependent properties in the table. Based on a simplified moving heat source model in (9), the product $K\ C_p\rho$ is inversely related to the maximum temperature on the idealised "tool-work interface" so this is also shown in table 2. The properties can be compared with the DTC designated titanium alloy (24, 25), which will also be used as a baseline material in the experimental programme below. Based on the tabulated values it would be expected that the Co-Cr-Mo materials would qualify as a DTC material given the higher strength and hardness. By comparison, the product $KC_p\rho$ is lowest for titanium which is well known to exhibit relatively high temperatures during cutting. The consequent high rate of tool wear variation with cutting speed, also serves to classify titanium as a difficult-to-cut material. However,

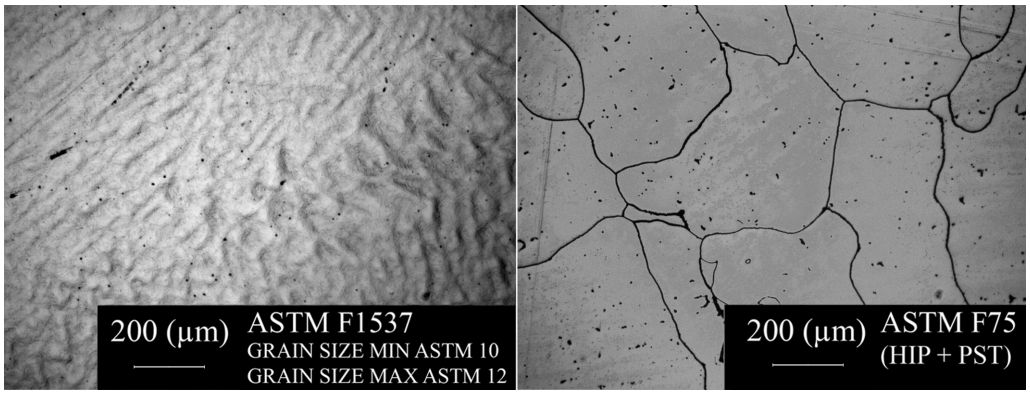

Figure 3: Microstructure of two Co-Cr-Mo alloys.

Property	Units	ASTM F1537(22) Co-Cr-Mo	ASTM F75(5) Co-Cr-Mo	ASTM F136 (21) Ti-6Al-4V
Tensile Strength	MPa	1403	920	940
0.2% Proof Stress	MPa	928	527	870
Elongation	%	29	16.5	16
Young's Modulus	GPa	283	216	114
Hardness	HRC	40	34	31
Thermal Conductivity (k)	$W \cdot m^{-1}K^{-1}$	14.8	13	7.2
Specific Heat Capacity (C_p)	$J \cdot Kg^{-1}K^{-1}$	452	450	560
Density (ρ)	$Kg \cdot m^{-3}$	$8,250$	$8,300$	$4,420$
Thermal Diffusivity	$m^2 s^{-1}$	$3.72 \cdot 10^{-6}$	$3.00 \cdot 10^{-6}$	$2.91 \cdot 10^{-6}$
$k \cdot C_p \cdot \rho$	$Kg^2 s^{-5} K^{-2}$	13.91	11.21	7.20

Table 2: Mechanical Properties of biomedical alloys ASTM F75 ASTM F1537 and ASTM F136 alloys

the values of this product for ASTM F1537 and F75, at about double the value for titanium, should be compared with 1020 steel and 75ST aluminium at about 4 and 5 times this baseline value respectively. But the subject of this paper is to determine the effect of fundamental parameters on forces and power in cutting of Co-Cr-Mo F75 alloy and, more generally, to elucidate the mechanisms of chip formation and material removal. The experimental programme now follows and the results will be later referenced to the tabulated properties as part of the subsequent analysis and discussion.

3. Experimental Programme

A specific objective of the experimental programme described now is to investigate the effect of the two most fundamental parameters, cutting speed (v_c) and undeformed chip thickness (h), on the two force components, the thrust force (F_t) and feed force (F_f) in two dimensional orthogonal cutting. This will enable a determination of "Kienzle coefficients" for this set-up and a more universal comparison with coefficients for other materials.

3.1. Experimental Plan and Design

The implemented control parameters and values in this full factorial experiment are shown in Table 3 with the number of repeat test runs shown as the table entry.

		Undeformed Chip Thickness $h(\mu m)$						
		20	40	60	80	100	120	140
Cutting Speed	20	2	1	1	2	2	1	2
$v_c(mmin^{-1})$	40	2	2	3	2	2	2	2
	60	2	1	2	1	2	1	2

Table 3: Experimental Control Parameters and the Number of Test Runs (actual).

3.2. Experimental Set-up and Equipment

The experiments were carried out on a precision HAAS TL2 CNC lathe with an 8.9 kW spindle motor

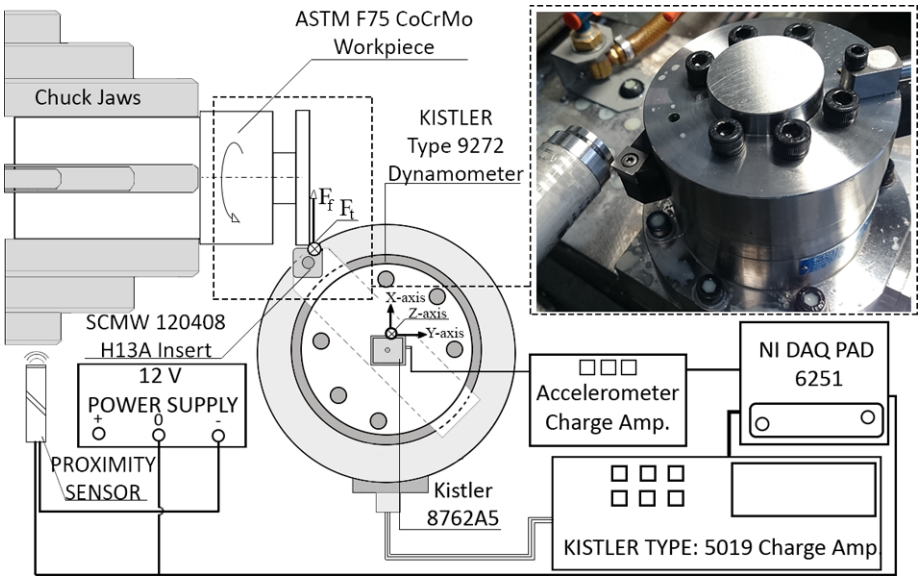

Figure 4: Schematic and Inset Photograph of Experimental Set-up.

rated for a maximum speed of 2000 RPM and driving a 208 *mm* capacity chuck with maximum cutting length of 1.22 *m* between centres. The set-up for the experiments involved the design of a rigid tool-holding fixture, as shown in figure 4 mounted on a 4 component Kistler type 9272 dynamometer with 50019 charge amplifier. The fixture design was analysed by FEA for stiffness in the direction of thrust force (F_t) and feed force (F_f), and found to be 148 and 181 Nmm^{-1} respectively. A modal analysis of this assembly with infinite base rigidity showed the lowest natural frequency to be 3.6 kHz, well above the lowest dynamometer in-plane natural frequency of 1.5 kHz. The full range specification for the three component dynamometer was 5, 5 and 20 kN for X, Y and Z directions as shown in figure 4. The transducer linearity and hysteresis is less than 1% of full scale operation in all ranges with sensitivities in X, Y and Z directions of -7.94, -7.92 and -3.62 pC/N. The dynamometer was cross-calibrated off the machine on a Hounsfield tensometer and found to conform within 5% of the Hounsfield measurements over the range from 0 to 4kN. The obtained results for Ti-6Al-4V (F136) were also compared with reported results in (26) and found to be comparable. The set-up further involved the installation of a Kistler 8762A5 accelerometer, with Wilcoxon Research P704B charge amplifier, as shown in figure 4. It was used to monitor the onset of any chatter during the experiments. Furthermore, a proximity sensor was also fitted, as shown in figure 4, enabling measurement of the actual number of rotations and rotational speed of the chuck, and synchronisation with the measured forces during each test run. Noting the kinematics of the orthogonal cutting set-up on the machine (as described below), measurement of the total depth of cut, by diameter measurements before and after each test run, provided verification of the programmed machine infeed and infeed per rotation and thus a measurement of the actual undeformed chip thickness. The output from the charge amplifier for the Kistler dynamometer, the accelerometer and the proximity sensor was connected to a National Instruments PAD 6251 data acquisition system. The DAQ system was connected to a PC with LabView 2014 software. The output was recorded against the same time channel, the data being sampled at 150 KHz. The force data was analysed using NI DiaDem 2014 software including low-pass digital filtering of 1.5 kHz prior to evaluation of the averages of the force component during steady state cutting.

3.3. Fixed Process Parameters

The fixed process parameters are shown in table 4. The physical and mechanical properties of the work material and the effect of the production processes on these, and the evolution of the micro-structure, have been described in the literature review. The Co-Cr-Mo work material used was supplied by DePuy Synthes in conformance with the ASTM 75 standard. After investment casting of the round bar, the microstructure and properties were modulated by Hot Isostatic Pressing and Partial Solution Treatment. The workpiece characteristics

were validated in part by metallographic examination and hardness measurements taken at intervals in the radial and axial directions; the microstructure of the alloy is shown on figure3, the nominal mechanical proeprties are listed in table 2 and the mean measured hardness value is as shown in table 2. The test bars were pre-machined on the HAAS CNC lathe to provide a precision cylindrical surface with submicron run-out. The pre-machined bar was then turned to form 3mm wide lands for the orthogonal cutting test runs; the land width being determined to ensure plain strain conditions. The tungsten carbide insert type described in the table 4 is one used commonly in industry for cutting Co-Cr-Mo alloys; the effect of tool wear as a noise parameter is obviated or minimised by using unworn edges for each test run. The basic cutting tool angles and geometric parameters for orthogonal cutting are given; the edge radius value shown is an average from measurements using a Keyence VHS-2000 microscope. The machine was charged with the indicated soluble oil coolant at the concentrations shown. The coolant was delivered through single nozzle directed at the rake face of the tool at $\approx 45^{\circ}$ with specified flow rate.

4. Experimental Procedure

The procedure followed in each test run involved initial measurement of the outside diameter of the pre-machined bar on the lands and setting accordingly of the CNC parameters for the specific test conditions, including; the initial tool position, the total infeed and linear speed (v_c) which provided the CNC control with the required input to enable control of the spindle speed as a function of the changing work diameter. The settings thus provide both the fundamental speed and undeformed chip thickness (UTC) according to the two factor experimental design but also ensure that the duration of the engagement involves multiple rotations (minimum of 5) and stabilisation of the force component profiles in each engagement. After the test run, a measurement of the bar diameter is repeated and the actual UCT is easily calculated from the number of rotations recorded as pulses by the aforementioned monitored proximity sensor. The statistics used for the purpose of the presentation of results here is the average of the two force component in a run (both F_f and F_t) and the range of the averages where test runs are repeated.

5. Results

The measured average feed force (F_f) and thrust force (F_t) values for Co-Cr-Mo F75 are shown in figures 5 and 6 as a function of the undeformed chip thickness (h) at three levels of cutting speed. The results are shown along with results for titanium Ti-6Al-4V, F136 at two speeds and UCT values in a reduced range. A two way analysis of variance (ANOVA) for the Co-Cr-Mo results shows a statistically significant variation for both force components with respect to both independent parameters at a 99% level of confidence. However, the test statistic for F_t was only marginally greater than the critical value (both independent parameters) at the 99% level of confidence, while the correlation for F_t was shown to be even statistically significant at a 99.9% level. A linear regression analysis of the results for the cutting force component, at each of the three speed levels separately, showed correlation or R-squared coefficients which exceeded 0.99 in all cases. However, the correlation coefficients were not as high for the feed force component as a function of UCT, being 0.59, 0.95 and 0.98 at the cutting speeds of 20, 40 and 60 m/min. respectively. It is surmised from inspection of both figures 5 and 6, but 6 in particular, that there is a transition in the $F_t \rightarrow$h characteristic between the UCT values of 60 and 80 μm at the intermediate speed of 40 m/min. In view of this and in the context of a high level of statistical confidence in the linear regression results, test runs were repeated at reduced intervals between these UCT values (specifically at 62,65,68,71 and 76 μm) as also shown in figures 5 and 6. These repeat results confirm the transitions again noting that values before and after practically align with the values at the lower and higher cutting speeds. This transition is discussed later.

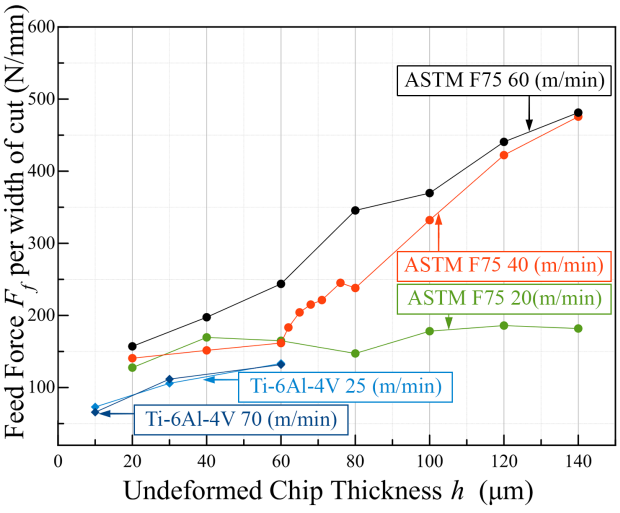

Figure 5: Feed Force F_f per Width of Cut vs. Undeformed Chip Thickness.

Test Parameter	Units:	Value:
Work Material:		
Material properties:		See Table 2
Stock Shape Dimensions	*mm*	ASTM F75 Φ 60 Round bar ASTM F136 Φ 110 Round bar
Measured Hardness:	HV(HRC)	322(34) for ASTM F75
Microstructure:		See Figure3
Width of Land:	mm	3
Tool Geometry		
Insert Code:	N/A	SCMW 120408 H13A
Rake Angle:	°	0
Relief Angle:	°	7
Cutting Edge Radius, r_β:	μm	14
Coolant		
Coolant Type:	N/A	FUSCH ECOCOOL ULTRALIFE A
Coolant Flow:	$l \cdot min^{-1}$	2.5
Coolant Concentration:	%	8.5

Table 4: Detailed List of Fixed Experimental Parameters.

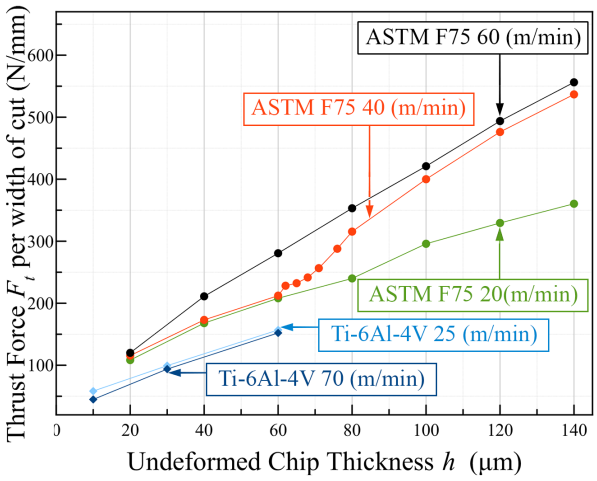

Figure 6: Thrust Force F_t per Width of Cut vs. Undeformed Chip Thickness.

6. Discussion

The results presented in figure 5 and 6 show that the cutting forces in orthogonal cutting of Co-Cr-Mo are significantly higher than in cutting of medical grade titanium over the common range as shown. This varies from 38 to 60 % at 20/25 m/min, and 60 to 83% at 60/70 m/min over the range from 20 to 60 μm UCT. Clearly, this does not correlate with the difference in yield and proof stress under ambient conditions. Moreover, a difference is evident in the effect of speed where the titanium alloy is unaffected, while the Co-Cr-Mo alloy exhibits a clear effect of speed and a difference in the cutting coefficient as suggested by the slope difference. The specific cutting forces for F75 were also greater than for the warm worked F1537 Co-Cr-Mo by between 20 and 41% at the cutting speed of 60 m/min and over the wider range between 20 to 80 μm UCT respectively. This is based on the results reported in (6); it is also noted that there was a lesser effect of speed on the warm worked F1537 alloy. The effect of speed for Co-Cr-Mo F75 may indicate a strain rate dependency if the results for the extreme speeds only are considered (increasing proportionately with UCT). However, the results at the intermediate speed of 40 m/min in figure 6, shows a confirmed transition between UCT values of 60 and 80 μm, indicating also a discontinuous rather than continuous effect of speed. The examination of the chip morphology did not provide any further insight as to the possible cause. One proposed hypothesis is that this transition may be due to the breakdown of a built-up edge as investigated by (27, 28) for other materials. This will be the subject of future research. Where, F_t is the specific thrust force (measured cutting force component per mm width of land, b, here), $k_{(c1.1)}$ is the unit specific cutting force coefficient in MPa (k_c measured at (h) =1 mm), h is in mm, and m_c is the slope of $k_c$vs h on a log-log plot. Figure 7 thus represents the basic nonlinearity of the thrust force as a function of the UCT (h) on a log-log plot for the cutting speeds of 20 and 60 m/min. Thus the Kienzle equation and coefficients have been obtained for this Co-Cr-Mo F75 material in orthogonal cutting and may be used for accurate predic-

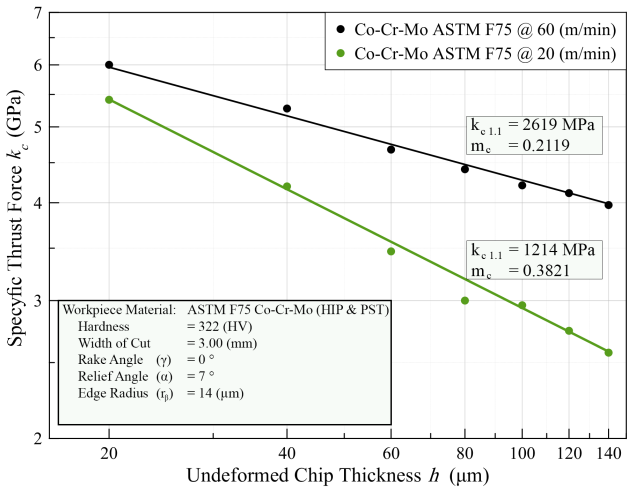

Figure 7: Kienzle Specyfic Thrust Force Coefficient for ASTM F75 Co-Cr-Mo

tion of cutting forces. Again, the equations to be used depend on the cutting speed as shown. Future research will investigate the "transition region" in order to confirmed the hypothesis that the transition is related to a physical parameter and criterion, such as a critical level of mechanical power input.

An alternative approach, proposed by Altintas and others (29), is to assume that the cutting forces vary linearly with the UCT in the range and determine the cutting coefficients according to (29):

$$\begin{cases} F_t = K_{tc} \cdot b \cdot h + K_{te} \cdot b \\ F_f = K_{fc} \cdot b \cdot h + K_{fe} \cdot b \end{cases} \quad (2)$$

Where Altintas describes the K_{te} and K_{fe} as the edge / ploughing coefficients and K_{tc} and K_{fc} as the cutting coefficient (for the thrust and feed components respectively)

These cutting force coefficients are the best-fit line coefficients (intercepts and slopes) for the two force components as shown in table 6 noting again the boundary conditions that apply in the parameter space resulting in two sets of coefficients.

In order to evaluate the average shear stress τ_s in the primary shear zone, a value of the shear plane angle Φ is required. This is typically obtained via measurement of the chip compression ratio. However, examination of chip morphology in orthogonal cutting of Co-Cr-Mo alloy, have shown formation of shear localised "saw-tooth" chip. The detailed characterisation of chip morphology and the shear plane angle will be described in follow-up publication.

	Thrust Components		**Feed Components**	
v_c	K_{tc}	K_{te}	K_{fc}	K_{fe}
(m/min)	(N/mm^2)	(N/mm)	(N/mm^2)	(N/mm)
20	2084.3	77.5	372	135.25
60	3597.1	60.2	2829.6	93.0

Table 5: Ploughing and cutting coefficients for two speeds

7. Conclusions

The main objective of the research reported in this paper was to determine the effects of the most basic parameters, v_c and h on the force components in orthogonal cutting of the important medical grade Co-Cr-Mo ASTM F75 alloy. The cutting speed was varied over a wide range for this alloy, encompassing the typical working range, while the undeformed chip thickness levels included the Kienzle mid-range" from 10 to 100 μm. A comparison of the results with the more common titanium Ti-6Al-4V alloy showed that the feed and thrust force component levels were higher in both cases. Analysis of the results demonstrated a statistically significant increase in both component force levels with undeformed chip thickness and cutting speed. Omitting the results for the intermediate speed level, linear regression at the extreme speeds showed an excellent fit. At the intermediate speed, there was a transition between 60 and 80 μm; an effect that was confirmed in a repeat experiment. The cause of this is unknown but one hypothesis proposed here is that the phenomenon is related to the breakdown (or formation) of a built-up edge, related in turn to a threshold mechanical power input. Above and below this threshold, the force components may be independent of cutting speed, as essentially found for titanium here. The underlying mechanism and the conditions for the onset of this transition will be the subject of future research.

This paper also determines the Kienzle equation coefficients for this Co-Cr-Mo ASTM F75 alloy in the examined range of cutting speeds and UCT levels with two sets of coefficients due to the identified transition. Similarly, "constant" cutting coefficients are also determined for use in the standard approach applied by other Researchers and enabling future use in macro-mechanics models of more complex cutting processes such as milling.

8. Acknowledgements

We would like to thank DePuy Synthes and Enterprise Ireland for supporting this research through the

Innovation Partnership (IP) programme. The Innovation Partnership programme which is co-funded by the European Union through the European Regional Development Fund 2014-2020.

References

[1] D. F. Williams, On the mechanisms of biocompatibility, Biomaterials 29 (2008) 2941–2953.

[2] DePuy, Synthess, Attune knee system, 2016.

[3] CDC, Cost of hospital discharges with common hospital operating room procedures in nonfederal community hospitals, by age and selected principal procedure: United states, selected years 20002012, 2014.

[4] J. Tozzi, Older, heavier americans fuel a 4 billion knee replacement market, 2015.

[5] R.Kaiser, Study of the Effect of Casting Variables and Heat Treatment Procedure on the Microstructure and mechanical Properties of Co-Cr-Mo Biomedical Alloy, Thesis, 2013.

[6] W. Chen, Cutting forces and surface finish when machining medium hardness steel using cbn tools, International Journal of Machine Tools and Manufacture 40 (2000) 455–466.

[7] N. R. Dhar, M. Kamruzzaman, M. Ahmed, Effect of minimum quantity lubrication (mql) on tool wear and surface roughness in turning aisi-4340 steel, journal of materials processing technology 172 (2006) 299–304.

[8] S. Baron, E. Ahearne, An investigation of force components in orthogonal cutting of medical grade cobalt chromium alloy (astm f1537), Proceedings of the Institution of Mechanical Engineers, Part H: Journal of Engineering in Medicine, Submitted for Publication in 2016. 16 (2015).

[9] S. Baron, E. Ahearne, P. Conolly, S. Keaveney, G. Byrne, An assessment of medical grade cobalt chromium alloy astm f1537 as a difficult to cut (dtc) material, 2015.

[10] A. Jabbari, S. Youssef, Physico-mechanical properties and prosthodontic applications of co-cr dental alloys: a review of the literature, The journal of advanced prosthodontics 6 (2014) 138–145.

[11] C. Montero-Ocampo, R. Juarez, A. S. Rodriguez, Effect of fcc-hcp phase transformation produced by isothermal aging on the corrosion resistance of a co-27cr-5mo-0.05 c alloy, Metallurgical and Materials Transactions A 33 (2002) 2229–2235.

[12] K. Ishida, T. Nishizawa, The co-cr (cobalt-chromium) system, Bulletin of Alloy Phase Diagrams 11 (1990) 357–370.

[13] C. Sikkenga, C. A. Castings, Casting, vol. 15, ASM Handbook, ASM International (2008) 1114–1118.

[14] ASTM, International, Standards, Standard Specification for Cobalt-28 Chromium-6 Molybdenum Alloy Castings and Casting Alloy for Surgical Implants (UNS R30075)., ASTM International standards, ASTM International, 2012.

[15] F. R. M. Limited, Astm f1537 warm worked billet- metallurgical certificate of conformity, 2011.

[16] R. Liu, S. Q. Xi, S. Kapoor, X. J. Wu, Investigation of solidification behavior and associate microstructures of cocrw and cocrmo alloy systems using dsc technique, Journal of Materials Science 45 (2010) 6225–6234.

[17] J. R. Davis, Nickel, cobalt, and their alloys, ASM international, 2000.

[18] Y. Bedolla-Gil, M. Hernandez-Rodriguez, Tribological behavior of a heat-treated cobalt-based alloy, Journal of materials engineering and performance 22 (2013) 541–547.

[19] M. Mori, K. Yamanaka, S. Sato, K. Wagatsuma, A. Chiba, Microstructures and mechanical properties of biomedical co-29cr-6mo-0.14n alloys processed by hot rolling, Metallurgical and Materials Transactions A 43 (2012) 3108–3119.

[20] J. A. Disegi, R. L. Kennedy, R. Pilliar, Cobalt-base alloys for biomedical applications, ASTM West Conshohocken, PA, ????

[21] S. Sun, M. Brandt, M. Dargusch, Characteristics of cutting forces and chip formation in machining of titanium alloys, International Journal of Machine Tools and Manufacture 49 (2009) 561–568.

[22] Sandvik, Inspection certificate according to bs en 10204.3.1 of diameter co/cr warm worked of astm f1537 standard 2008 uns r31537, 2012.

[23] M. C. Shaw, Metal cutting principles, volume 2, Oxford university press New York, 2005.

[24] E. Ezugwu, J. Bonney, Y. Yamane, An overview of the machinability of aeroengine alloys, Journal of materials processing technology 134 (2003) 233–253.

[25] E. O. Ezugwu, Z. M. Wang, Titanium alloys and their machinabilitya review, journal of materials processing technology 68 (1997) 262–274.

[26] M. Cotterell, G. Byrne, Characterisation of chip formation during orthogonal cutting of titanium alloy ti6al4v, CIRP Journal of Manufacturing Science and Technology 1 (2008) 81–85.

[27] N. Fang, P. Dewhurst, Slip-line modeling of built-up edge formation in machining, International Journal of Mechanical Sciences 47 (2005) 1079–1098.

[28] Childs, T. H. C., Developments in simulating built up edge formation in steel machining, Procedia CIRP 1 (2012) 78–83.

[29] Y. Altintas, Manufacturing automation: metal cutting mechanics, machine tool vibrations, and CNC design, Cambridge university press, 2012.